Available online at www.sciencedirect.com
ScienceDirect
Journal of Computational Physics 227 (2007) 1162–1175
JOURNAL OF COMPUTATIONAL PHYSICS
www.elsevier.com/locate/jcp

Modeling and simulation of Li-ion conduction in poly(ethylene oxide)

L. Gitelman [a], M. Israeli [b,✠], A. Averbuch [c,*], M. Nathan [d], Z. Schuss [e], D. Golodnitsky [f]

[a] *Faculty of Applied Mathematics, Technion, Haifa 32000, Israel*
[b] *Faculty of Computer Science, Technion, Haifa 32000, Israel*
[c] *School of Computer Science, Tel Aviv University, Tel Aviv 69978, Israel*
[d] *School of Electrical Engineering, Tel Aviv University, Tel Aviv 69978, Israel*
[e] *School of Mathematical Sciences, Department of Applied Mathematics, Tel Aviv University, Tel Aviv 69978, Israel*
[f] *School of Chemistry, Tel Aviv University, Tel Aviv 69978, Israel*

Received 8 May 2007; received in revised form 29 August 2007; accepted 31 August 2007
Available online 14 September 2007

Abstract

Polyethylene oxide (PEO) containing a lithium salt (e.g., LiI) serves as a solid polymer electrolyte (SPE) in thin-film batteries and its ionic conductivity is a key parameter of their performance. We model and simulate Li^+ ion conduction in a single PEO molecule. Our simplified stochastic model of ionic motion is based on an analogy between protein channels of biological membranes that conduct Na^+, K^+, and other ions, and the PEO helical chain that conducts Li^+ ions. In contrast with protein channels and salt solutions, the PEO is both the channel and the solvent for the lithium salt (e.g., LiI). The mobile ions are treated as charged spherical Brownian particles. We simulate Smoluchowski dynamics in channels with a radius of ca. 0.1 nm and study the effect of stretching and temperature on ion conductivity. We assume that each helix (molecule) forms a random angle with the axis between these electrodes and the polymeric film is composed of many uniformly distributed oriented boxes that include molecules with the same direction. We further assume that mechanical stretching aligns the molecular structures in each box along the axis of stretching (intra-box alignment). Our model thus predicts the PEO conductivity as a function of the stretching, the salt concentration and the temperature. The computed enhancement of the ionic conductivity in the stretch direction is in good agreement with experimental results. The simulation results are also in qualitative agreement with recent theoretical and experimental results.

Keywords: Thin-film batteries; Conduction in a single PEO molecule; PEO conductivity; Brownian particles; Smoluchowski dynamics

* Corresponding author. Tel.: +972 54 569 44 55; fax: +972 151 54 5694455.
E-mail address: amir@math.tau.ac.il (A. Averbuch).
✠ Prof. Moshe Israeli passed away on February 18, 2007. This paper is dedicated to his memory.

0021-9991/$ - see front matter
doi:10.1016/j.jcp.2007.08.033

1. Introduction

Lithium and lithium-ion batteries have made substantial and significant gains in the last 30 years, becoming the dominant rechargeable batteries for consumer portable applications. A lithium-ion battery employs a metal oxide or sulfide material with typically a layered structure (such as $LiCoO_2$, $LiMn_2O_4$, $LiNiO_2$, TiS_2, etc.) as its positive electrode (cathode). The negative electrode (anode) is typically a graphitic carbon. During discharge, the positive material is reduced and the negative material is oxidized. In this process, lithium ions are de-intercalated from the anode and intercalated into the cathode material. The charge/discharge voltage depends on the current and resistance of all battery components.

In most solid-state lithium-ion batteries, a thin-layer (0.02–0.2 mm) solid polymer electrolyte (SPE) is sandwiched between two electrodes and the ionic conductivity of the SPE medium is of prime importance. A classical SPE consists of organic macromolecules (usually of a polyether polymer) doped with inorganic salts. In order to form an effective SPE with mobile cations, a balance must be struck in a cation–polymer bond so that it is sufficiently strong to promote salt dissociation, but sufficiently weak to permit cation mobility. Poly(ethylene oxide) (PEO) is a classic example of a lithium ion–host matrix because of a peculiar array in the $(–CH_2–CH_2–O–)_n$ chain that provides the ability to solvate low-lattice-energy lithium salts. The typical molecular weight of the PEO is 5×10^6, implying $\sim10^5$ $O(CH_2)_2$ repeat units per molecule.

Pure PEO near room temperature contains both amorphous and crystalline microphases, and has an extended helical structure with seven $O(CH_2)_2$ groups in two turns of the helix [1,2]. This long helical chain is bent many times. The incorporation of salts into the polymer inevitably reduces the freedom of polymer-chain motion via binding interactions between the ether oxygens and cations. In this case, the anion is dissociated from the cation and does not interact significantly with the chain. Its motion requires a free volume between the polymer chains [4].

It is well established that cation transport occurs primarily along the helical axis [1,2]. Obviously, this venue of ionic motion cannot alone account for transporting ions over long distances, because the polymer molecule is extremely entangled and it is sometimes energetically more beneficial for an ion to jump to another molecule than to continue its motion by a more complicated route. Therefore inter-chain transport is essential for long-range conduction. It has recently been found [5–8] that intra-chain transport is far more efficient than inter-chain hopping, making the latter process rate- limiting. The inter-chain ion hopping is assisted by a polymer segmental motion that controls the instantaneous distance between adjacent chains. The fact that such moves are essential for long-range transport through the polymer network explains the strong correlations usually observed between ionic conduction and host segmental dynamics in these systems, e.g., the correlation between ionic mobility and the host glass transition [5].

It has been shown in a series of recent articles [6–8] that stretching films of Li–P(EO) complexes results in a more than an order of magnitude enhancement of the DC conductivity along the stretch direction.

The following is a detailed summary of some experimental observations related to PEO stretching.

Refs. [6–8] discuss PEO–lithium salt polymer electrolytes LiX:P(EO)*n* with ethylene oxide-to-salt molar ratio *n* (i.e. the variable *n* indicates that for each Li^+ ion there are *n* atoms of "O" in the PEO polymer electrolytes) varying from 3 to 100. X represents different anions, such as iodide, triflate, hexafluoroarsenate, etc. The polymers were cast and hot pressed to be 300 μm-thick films. The length of the neck was 14 mm and its minimal internal width was 8 mm. The cross-section of the film at the neck was 0.3×8 mm^2. Films were stretched by applying a load along the stretching direction. Up to an extension load of 400 N/cm^2 along the polymer specimen, neither polymer electrolyte resistance nor visible sample changes were observed. Under a load of 450–800 N/cm^2, the samples began to flow and the DC conductivity increased by a factor of 2–40, depending on the EO:Li ratio (*n*) and stretching conditions. After removal of the load, stretched polymer electrolytes retained high ionic conductivity. In room temperature stretching, the length of the LiI:P(EO) polymer electrolyte films with $n = 20$ increased in the stretching direction by a factor of 2.5, whereas the width and the thickness decreased by a factor of 1.5 and 3, respectively. The changes in the dimensions of the films were much stronger when stretching was carried out at 60 °C. The DC conductivity in the stretching direction increased by a factor of 5–8 at $T = 40$ °C and by factor of 11–20 at 60 °C.

For films subjected to a critical load flowed, the film length increased by a factor of 3–6, whereas its thickness decreased by a factor of about 4.

The profound effect of stretching on the ion transport properties of polymer electrolytes was detected for different lithium salts, such as lithium iodide, lithium trifluoromethanesulfonate, lithium hexafluoroarsenate, lithium bis(oxalato)borate and lithium trifluoromethanesulfonimide. In [6] it was found experimentally, that there are at least three degrees of stretching-induced structural long- and short-range order. SEM, AFM and XRD tests detected a formation of unidirectionally oriented microphases, with each domain composed of aligned fibers. Detected changes in Fourier transform infrared spectroscopy were mainly related to the perturbation of the CH_2 groups and –O–C–C–O– torsional angles. It was suggested that stretched polymers adopt a modified helical structure, similar to that of an extended salt-free PEO helix. In [5] the authors presented a model that accounts for stretching-induced structural anisotropy accompanied by ion conduction enhancement. The authors addressed a transition from spherical to spheroidal shapes of the high conduction regions as a result of alignment.

This situation is similar to that in protein channels of biological membranes [9–12], where ions diffuse through a channel that separates two baths of salt solutions of different concentrations. In our case however, the bath solutions are replaced by a solid anode and cathode and the LiI salt is solvated in the dry polymer. Continuum models of the motion of ions through protein channels are most commonly based on the assumption of Brownian motion (diffusion) in an electric field, created by the 'permanent' charge of the protein, the charge of the mobile ions, and the voltage applied across the membrane [10,11]. These models are based on the mean-field assumption and need special assumptions to account for ion–ion interactions, such as finite ionic size.

The need for coarse-grained mathematical descriptions of ions in PEO/(channels) is apparent. A set of theories is needed to form a hierarchy of models using the following descriptions:

1. Atomic resolution theories are needed for small molecular dynamics (MD)simulations of ions and PEO/(channel) to capture the essential physics of permeation.
2. Brownian resolution theories are needed for coarser MD or Langevin simulations of ions in PEO.
3. Continuum theories are needed for coarser description of ions in PEO/(channel), involving only a small number of continuum variables, such as dielectric constants, diffusion coefficients, charge densities, electrostatic potentials and other averaged interaction forces.

The description (1) of ions in PEO/(channels) on the atomic level is derived from classical electrostatics [18] and mechanics [19]. The collective motion of all atoms and molecules at this level of resolution is described by a large number of ordinary differential equations coupled to Poisson's equation for the electrostatic field, as done in MD simulations [12]. The limitation of this description is obvious: there is not enough computational power available now or in the foreseeable future to keep track of all the relevant degrees of freedom for sufficiently long times to move an ion from anode to cathode by crossing the channel.

Descriptions (1) and (2) can be used to describe and model diffusion of interacting particles, however, as mentioned above, description (3) cannot capture finite size effects for ionic diffusion in confined geometries in a systematic way. We adopt therefore the Brownian resolution theory (2), which can handle the ion–ion interactions yet is computationally feasible. In the present setup, the I^- and Li^+ ions are kept apart from each other by the polymer and the Li^+ ions are kept apart by Coulombic repulsion, so the finite size effects become significant only at high concentrations. Therefore, we do not incorporate finite size effects in the present simulation, but we will investigate their effect in a subsequent paper.

In the coarsest Brownian resolution, we approximate the potential of the electric forces by Coulomb's potential of all mobile and fixed charges in the model and the applied potential, neglecting induced surface charges at interfaces. We then compare the simulation results with those of experiments reported in [6–8].

The paper has the following structure. The model is described in Section 2. A fast algorithm for particle simulation is given in Section 3. Simulation results and their comparison with experimental results reported in the literature are described in Section 4.

2. The model

The simulations and modeling carried out in the present work are focused on the analysis of the conductivity enhancement induced by orientational distribution of helical segments of the molecular chain (from isotropic to non-isotropic) as a result of PEO stretching.

As noted above, the as-cast PEO under consideration consists of long helical molecule of randomly oriented molecules. In our model, the as-cast PEO configuration is essentially that of a bundle of straight chains inclined relative to the line perpendicular to electrodes A and K (a single chain bridging the gap) (see Fig. 1).

The angle of inclination α of each helix (molecule) is assumed to be a random variable, uniformly distributed in the interval $0 \leqslant \alpha \leqslant \pi/2$.

We assume that for $\alpha = 0°$, the main Li^+ transport mechanism is a process of diffusion and migration inside the channel. For channels parallel to the electrodes ($\alpha = 90°$), the main mechanism is inter-channel hopping, and for intermediate SPE chain geometries ($0° < \alpha < 90°$) the transport process is a mixture of the two. The anions diffuse outside the helices, due to the repulsive electrical forces of the permanent charges of the helix. The diffusive motion of both lithium and iodine ions in the polymer matrix is due to the thermal motion of the polymer segments and chains.

In a simplified one-dimensional Brownian model, the polymer is represented as a combination of charge distribution, noise and dissipation. The solenoidal PEO helix, Fig. 2, is replaced [17] with a sequence of 2294 units of CH_2–CH_2–O, seven units of CH_2–CH_2–O per two turns of the helix (see Fig. 2). The helix has a radius R centered on and orthogonal to the x-axis. The length of two turns is $d = 1.93$ nm. The units of CH_2 are at a distance $R = 0.1$ nm from the x-axis, and the units of O are at a distance $r = 0.04$ nm from the x-axis. Typical charge distribution values are $+0.245$ for a unit of CH_2 and -0.406 for a unit of O [15–17].

The Coulombic potential created on the x-axis by the PEO charges is given by

$$\Phi(x) = \sum_{j=1}^{N} \left(\sum_{i=1}^{n_1} \frac{q^+}{\sqrt{(x - x_{ij}^+)^2 + R^2}} + \sum_{i=1}^{n_2} \frac{q^-}{\sqrt{(x - x_{ij}^-)^2 + r^2}} \right), \tag{2.1}$$

where q^- and q^+ are the net negative and positive charges on a ring, x_{ij}^+ and x_{ij}^- are respectively the coordinates of the units CH_2 and O, and n_1 and n_2 are respectively the numbers of positive and negative particles, respectively. We assume an external applied potential $\Psi_E(x)$. The Coulombic potential of the inter-ionic forces acting on the nth lithium ion at x_n is given by

$$\Psi_{Li^+}(x, \boldsymbol{x}, \boldsymbol{y}) = \sum_{i \neq n} \frac{q_{Li^+}}{|x - x_i|} + \sum_{i=1}^{LN} \frac{q_{I^-}}{\sqrt{|x - y_i|^2 + R^2}} + \Phi(x) + \Psi_E(x) \tag{2.2}$$

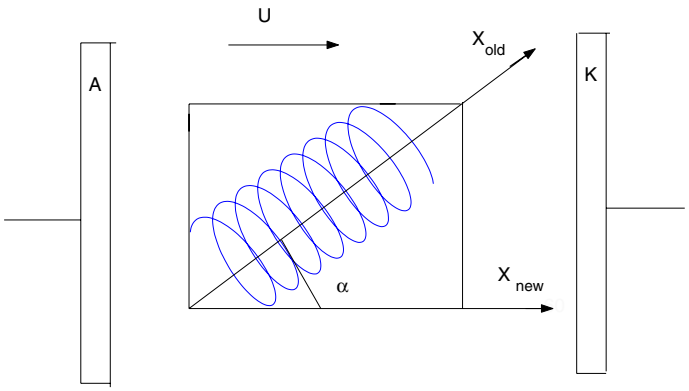

Fig. 1. The helix (molecule) and the setup of the physical model.

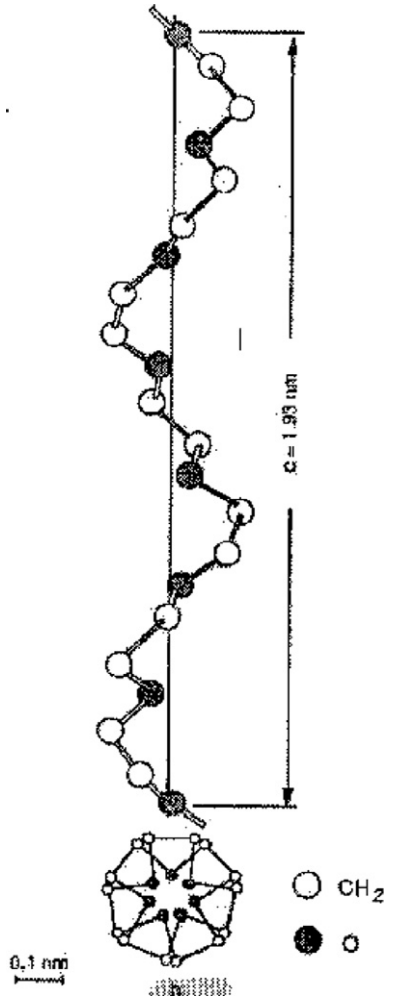

Fig. 2. Schematic model of poly(ethylene oxide). The same two turns of the helix appear at the bottom of the figure.

and that for the force acting on the nth iodine ion at y_n is

$$\Psi_{\mathrm{I}^-}(y,\boldsymbol{x},\boldsymbol{y}) = \sum_{i=1}^{LN} \frac{q_{\mathrm{Li}^+}}{\sqrt{|y-x_i|^2+R^2}} + \sum_{i\neq n} \frac{q_{\mathrm{I}^-}}{|y-y_i|} + \Phi(y) + \Psi_E(y), \tag{2.3}$$

where $\boldsymbol{x} = (x_1, x_2, \ldots, x_{LN})$, $\boldsymbol{y} = (y_1, y_2, \ldots, y_{LN})$ are the coordinate vectors of the lithium and iodine ions, respectively, in configuration space, $(i = 1, \ldots, NL)$. The random motion of the ions in the channel is described by the overdamped Langevin equations [12,14]

$$\begin{aligned} \gamma_{\mathrm{Li}}\dot{\boldsymbol{x}} &= \boldsymbol{F}_{\mathrm{Li}}(\boldsymbol{x},\boldsymbol{y}) + \sqrt{\frac{2\gamma_{\mathrm{Li}}kT}{m_{\mathrm{Li}}}}\dot{\boldsymbol{w}}, \\ \gamma_{\mathrm{I}}\dot{\boldsymbol{y}} &= \boldsymbol{F}_{\mathrm{I}}(\boldsymbol{x},\boldsymbol{y}) + \sqrt{\frac{2\gamma_{\mathrm{I}}kT}{m_{\mathrm{I}}}}, \dot{\boldsymbol{v}}, \end{aligned} \tag{2.4}$$

where $\dot{\boldsymbol{w}}$ and $\dot{\boldsymbol{v}}$ are vectors of independent standard δ-correlated Gaussian white noises, and the components of the electric forces (per unit mass) on the nth lithium and iodine ions, respectively, are given by

$$F_{\mathrm{Li}}^{(n)}(\boldsymbol{x},\boldsymbol{y}) = -q_{\mathrm{Li}^+}\frac{\partial\Psi_{\mathrm{Li}^+}(x,\boldsymbol{x},\boldsymbol{y})}{\partial x}\bigg|_{x=x_n}, \tag{2.5}$$

$$F_{\mathrm{I}}^{(n)}(\boldsymbol{x},\boldsymbol{y}) = -q_{\mathrm{I}^-}\left.\frac{\partial \Psi_{\mathrm{I}^-}(y,\boldsymbol{x},\boldsymbol{y})}{\partial y}\right|_{y=y_n}. \tag{2.6}$$

We simulate the system (2.4) by discretizing time and moving the ions according to the Euler scheme

$$\begin{aligned}\boldsymbol{x}(t+\Delta t) &= \boldsymbol{x}(t) + \frac{\boldsymbol{F}_{\mathrm{Li}}(\boldsymbol{x}(t),\boldsymbol{y}(t))}{\gamma_{\mathrm{Li}}}\Delta t + \sqrt{\frac{2kT}{\gamma_{\mathrm{Li}} m_{\mathrm{Li}}}}\Delta \boldsymbol{w}(t),\\ \boldsymbol{y}(t+\Delta t) &= \boldsymbol{y}(t)\Delta t\frac{\boldsymbol{F}_{\mathrm{I}}(\boldsymbol{x}(t),\boldsymbol{y}(t))}{\gamma_{\mathrm{I}}}\Delta t + \sqrt{\frac{2kT}{\gamma_{\mathrm{I}} m_{\mathrm{I}}}}\Delta \boldsymbol{v}(t),\end{aligned} \tag{2.7}$$

where $\Delta \boldsymbol{w}(t)$ and $\Delta \boldsymbol{v}(t)$ are zero mean independent Gaussian random variables with covariances $\boldsymbol{I}\Delta t$ ($\boldsymbol{I}$ is the unit matrix). A Li^+ trajectory $x_i(t)$ that reaches the graphite anode (on the right in Fig. 1) is instantaneously restarted at $x_i = 0$ and the counter of restarted trajectories is increased by 1. An I^- trajectory that reaches either the cathode or anode is instantaneously reflected. The total charge $Q(t)$ absorbed in the graphite by time t produces the noisy battery current

$$I(t) = \frac{\mathrm{d}Q(t)}{\mathrm{d}t}. \tag{2.8}$$

We simulate 16,058 bound ions in each chain [16]. The interactions between all charges are computed efficiently by a fast multipole method (FMM)-type method [20]. Our aim is to calculate the steady state average of $\langle I(t)\rangle$.

3. A fast algorithm for particle simulations

3.1. Potential computation

We assume that the diffusion of Li^+ ions through the channel is one-dimensional along the x-axis. The potential on the x-axis is given by Eq. (2.1) with $n_1 = 14$ and $n_2 = 7$. A straightforward direct summation of Eq. (2.1) requires $O(N^2)$ operations. We reduce the cost of evaluating these sums at each of the N target locations from $O(N^2)$ to $O(N)$ operations. In order to develop a fast algorithm, we first define the computational domain (also called "box") to be the smallest section of a helix that contains seven units of CH_2–CH_2–O. The origin of our system is the center of the domain (see Fig. 3), which coincides with the fourth particle O. The potential and the corresponding forces become periodic, $\Phi(x+d) = \Phi(x)$ and $F_{\mathrm{el}}(x+d) = F_{\mathrm{el}}(x)$, where d is the length of the domain (see Fig. 3). This approximation follows from the periodic structure of the polymer. We calculate the potential at a large number of points x inside one domain, taking into consideration only the contribution of several adjacent domains. The dependence of accuracy on the number of domains included in the computation is investigated below.

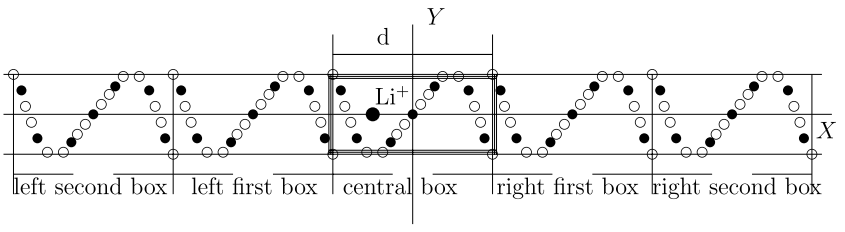

Fig. 3. The polymer chain is covered by N boxes. Each box contains 21 units of CH_2 and O. The origin is in the middle of the central domain. It coincides with the fourth particle O. The potential and the corresponding forces are periodic.

In order to perform the numerical computation of the potential, the polymer is covered by boxes. Each box contains 21 units of CH_2 and O (see Fig. 3). We assume that the boxes do not intersect each other and that the helix is infinitely long. The processing of remote areas of the polymer are considered below. The potential and the corresponding forces become periodic if we consider only an equal number of boxes on both sides of the central box. Therefore, instead of computing the mutual contributions of all the boxes in each computation, we only compute the coordinates of the Li^+ in the box that contains the origin of the coordinate system. We call this box a "*central*" box. We estimate the contribution to the potential and electrostatic forces in the central box from the boxes that lie on its left and right. The potential in the central box without the contributions from adjacent boxes on its left and right sides is denoted by Φ (can also be considered as Φ_0). The contribution from the first, second, third, forth boxes from the left and right sides of the central box is denoted by $\Phi_1, \ldots, \Phi_4$, respectively. The same type of notation applies to the electrostatic force F in the central box.

Fig. 4(top) shows the computed potential Φ (using Eq. (2.1), $N = 0$) in the central box without the contribution from adjacent boxes and Fig. 4(bottom) shows the contribution from boxes 1, 2, 3 and 4. The differences between the values of Φ and the values of Φ_1, Φ_2, Φ_3, Φ_4 are small but have to be considered. The differences give an indication that a small number of boxes (more than 4 but less than 10) are sufficient to increase the accuracy.

Fig. 5(top) shows the computed potential Φ in the central box (in percentage changes) from the contribution of three neighboring adjacent boxes ($N = 1, 2, 3$) and Fig. 5(bottom) shows the effect of adding a fourth box. The differences between the values of Φ and the values of Φ_1, Φ_2, Φ_3, Φ_4 are small but the differences have to be reduced. The relative changes (percentage-wise) in the potential are computed as follows. The potential in the *central* box is computed using the influence of the third box on each side. Then, we compute the potential in the *central* box using these boxes. We see from Fig. 5(top) that the contribution from the boxes beyond the third box on either side does not exceed ~7%. The contribution from the boxes beyond the fourth box on either side ~3.5% (Fig. 5(bottom)). The full description of the accuracy is given below.

Therefore, in order to obtain higher accuracy it is necessary to take more than four boxes ($N \geqslant 4$) on each side of the *central* box. More boxes on each side are needed to increase the accuracy by a factor of 10 when the

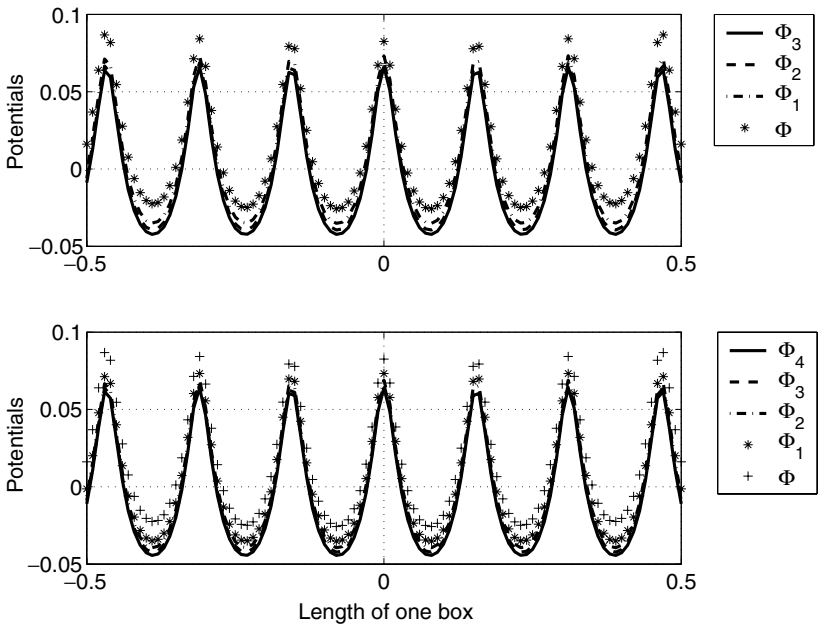

Fig. 4. Computation of the potential Φ (Eq. (3.1)) in the cental box. Top: without the contribution from adjacent boxes. The potential Φ_N, $N = 1, 2, 3$, in the *central* box includes the contribution from N left and right adjacent boxes. Bottom: the potential Φ_4 is computed in the *central* box taking into consideration the contribution from four left and four right adjacent boxes. The potential values are in the range between ~−0.05 and 0.09 non-dimensional units.

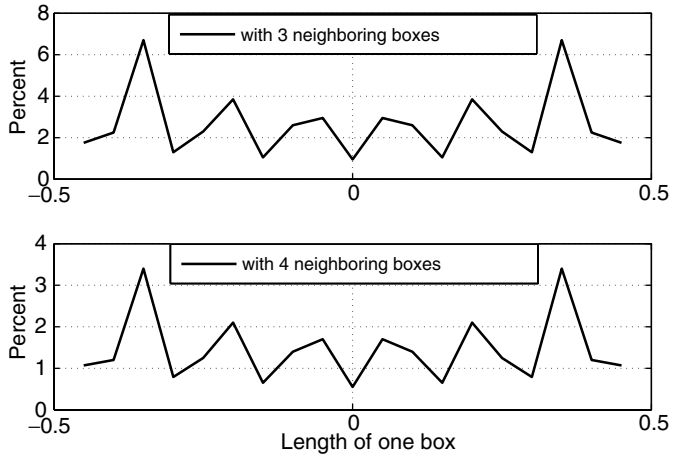

Fig. 5. The relative changes in the potential are expressed in percents. Top: computation with and without the contribution from the third left and third right adjacent boxes. This contribution does not exceed ~7%. Bottom: computation with and without the contribution of the fourth left and right adjacent boxes. This contribution does not exceed ~3.5%.

error is reduced to be below 3.5%. The contribution of these additional boxes beyond the fourth box on the *central* box is computed by using a Taylor expansion of the potential in Eq. (2.1) in powers of x. Therefore, we compute

$$\Phi_N(x) = \sum_{j=1}^{N} \left(\sum_{i=1}^{14} \frac{q^+}{\sqrt{(x - x_{ij}^+)^2 + R^2}} + \sum_{i=1}^{7} \frac{q^-}{\sqrt{(x - x_{ij}^-)^2 + r^2}} \right) + \phi(x), \tag{3.1}$$

where $\phi(x)$ represents the correction to the potential generated by charges contained inside remote adjacent boxes. Contribution from more distant boxes, beginning with the $N+1$th box, is represented by their Taylor approximation, as described below. The error will be reduced from 10^{-2} to 10^{-3} range by going from considering 4 boxes to 10 boxes.

As above, we compute the potential at p points in the *central* box to find its distribution. The same distribution is valid inside any other box, except for several boundary boxes, because the potential is periodic away from the boundaries. Then, we compute the coordinate of each Li^+ ion by Eq. (2.7). The Li^+ ion can be at any location in the polymer (in any box). If this ion is not located in the *central* box, we map its coordinates into the coordinates of the *central* box, as described below.

At this stage we ignore boundary effects. Therefore, the value of the potential repeats itself when we display the coordinate by an integer number of box lengths. We take advantage of this periodicity as follows. We perform a preliminary computation of $\Phi_N(x)$ at p points in the *central* box which requires $O(p)$ operations. To compute the potential at a given point x outside of the *central* box, we map its coordinate into the *central* box. In other words, we calculate an equivalent coordinate x_0 inside the *central* box where $x_0 = [x(\mathrm{mod})d] - d/2$, and d is the length of the *central* box. The value of the potential at the point x is equal to the value of the potential at x_0, which was computed above. This procedure is obviously inexpensive since it is done once.

3.2. Computing the forces

The electrostatic force on a Li^+ ion at a point x on the axis is given by Eq. (2.5). As for Φ, a straightforward direct summation in Eq. (2.5) requires $O(N^2)$ operations. We reduce the cost of evaluating these sums at each of the N target locations from $O(N^2)$ to $O(N)$ operations. We calculate the electrostatic force on a Li^+ ion, taking into consideration only the contribution from several adjacent boxes. The accuracy depends on the number of boxes included in the computation is investigated below.

The computation of the electrostatic force F is the same as was done for the potential. First, we compute the electrostatic force in the *central* box with the contribution from three left and right adjacent boxes ($N = 3$). Then, we compute a force F_4 on a Li^+ ion in the *central* box with the contribution from the four left and right adjacent boxes. The differences in the values of the forces are small on this scale. By going from F_3 to F_4 the accuracy gets better by a factor of 10 (see Fig. 8). The results are displayed in Fig. 6.

The relative changes of the force expressed in percentages is presented in Fig. 7 where the computation is done in a similar way to that of the potential above. Specifically, we compute the force in the central box without the contribution from the third left and the third right adjacent boxes. Then, we compute the force in the central box with the contribution from the third left and the third right adjacent boxes. We find that four boxes on each side of the central box are insufficient to achieve the required accuracy. Therefore, we consider the contribution from two additional boxes on each side. The results are displayed in Fig. 7.

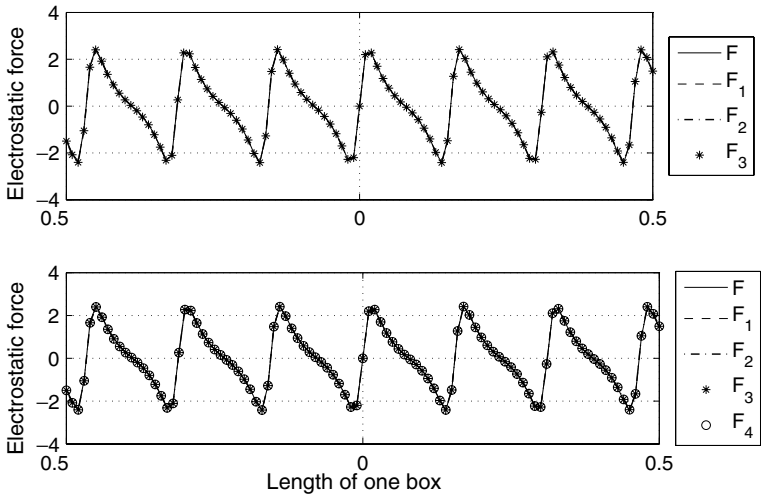

Fig. 6. Top: the electrostatic force F in the *central* box was computed without the contribution from adjacent boxes. The force F_N, $N = 1, 2, 3$, in the *central* box includes the contribution from N left and right adjacent boxes. Bottom: in addition to that, the force F_4 in the *central* box was computed with the contribution from *four* left and right adjacent boxes. The range of the forces is ~ -3 to 3 non-dimensional units.

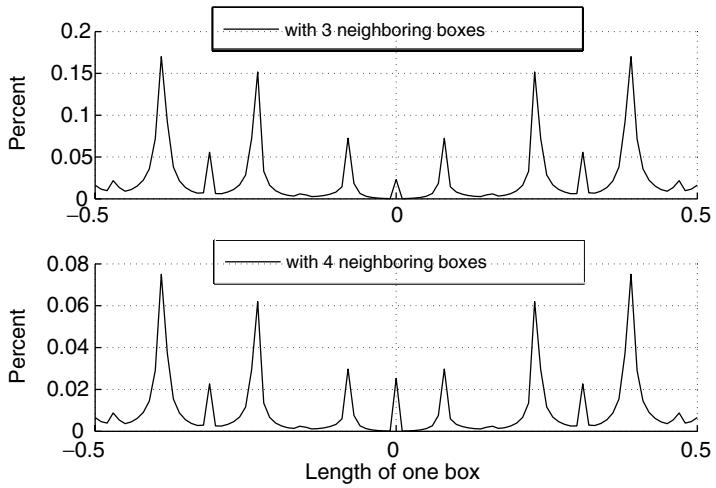

Fig. 7. The relative changes of the force expressed in percents. Top: computed with and without the contribution from the third left and the third right adjacent boxes. This contribution reaches up to $\sim$0.175%. Bottom: computed with and without the contribution from the fourth left and the fourth right adjacent boxes. This contribution reaches up to $\sim$0.08%.

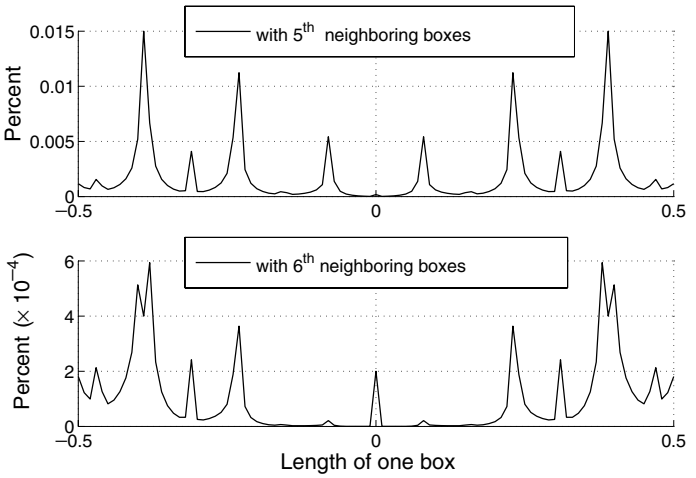

Fig. 8. The relative changes of the force expressed in percents. Top: computed directly with the contribution from five boxes on each side of central box. In addition, computation with four adjacent boxes on each side of the central box with an additional box. The computation uses Taylor expansions. The error between these two modes of computation reaches a maximum of 0.015% close to the boundary of the central box. Bottom: computed with and without the contribution from the sixth left and the sixth right adjacent boxes. This contribution is even less significant since it equals to $\sim 6 \times 10^{-4}\%$.

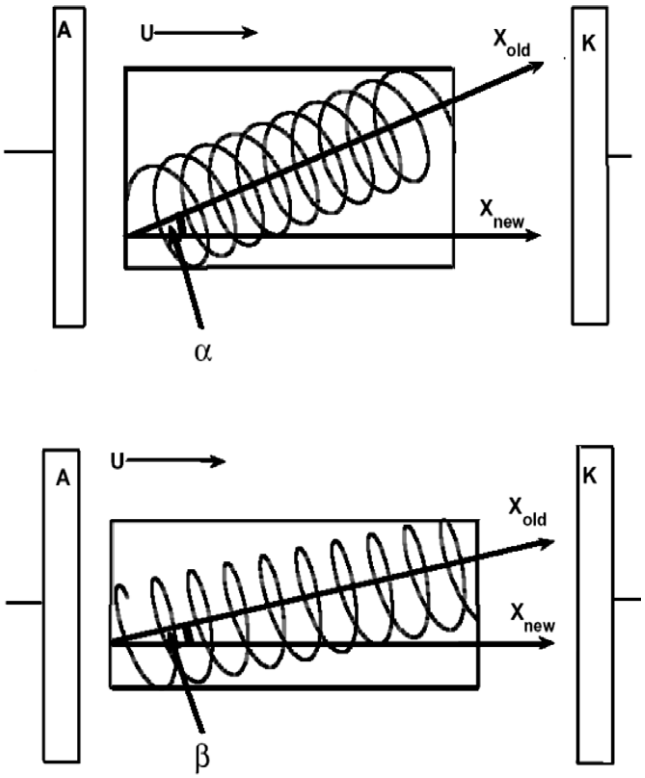

Fig. 9. Upon mechanical stretching, the molecular structures incline toward the stretching axis (X_{old}). Top: the mean angle of inclination of the molecule before the stretching α. Bottom: after stretching, the mean angle of inclination of the molecule decreases to $\beta < \alpha$. The length of the projection of the molecule on the axis X_{old} increases by a factor of 3–6, while its thickness decreases by a factor of roughly 4 (the length and the width of the rectangle is shown at the bottom (middle)).

Another force computation, which uses Eq. (2.6), is presented in Fig. 8. The error between the computations in the top and bottom parts of Fig. 8 reaches a maximum of 0.015% close to the boundary of the central box (see Fig. 8(top)).

In conclusion, from all the above computations, we will now base our force computations on the contribution from four adjacent boxes on each side of the central box with the Taylor expansions of two additional adjacent boxes. Therefore, Eq. (2.1) will assume $N = 4$.

4. Simulation results

4.1. Stretching by intra-box inclination of the polymer molecule

In our model (Section 2, Fig. 1), the polymeric film is a thin layer of molecular structures (boxes) that are oriented at random along an axis (X_{new}) where X_{new} is perpendicular to the electrodes A and K. In each box, each helix (molecule) forms a random angle with the X_{new} axis. Upon mechanical stretching, the helices align along the axis of stretching, i.e. the inclination of molecules decreases (see Fig. 9).

When the thickness of the film decreases and the helices are aligned along the stretching direction, the diameter of a single helix does not change.

The number of orientations along a chain molecule is large, so considering each of them individually is computationally expensive. Therefore, we adopt a statistical approach and calculate appropriate averages over a distribution of configurations of an ensemble of chain molecules.

In the model, we assume that stretching of the sample is achieved only by decreasing the inclination of a molecule inside a box. If the mean inclination of the molecule before stretching $\alpha_1 \simeq 1.2409738$ (Fig. 9(left)) drops to a value $\beta_1 = \arccos(3\cos\alpha_1) \simeq 0.2387879$ so that $\beta_1 = \arcsin(\frac{1}{4}\sin\alpha_1)$, then the film length L increases by a factor of 3, while its thickness d decreases by a factor of about 4. If the mean inclination of the molecule before stretching is $\alpha_2 \simeq 1.40857$ (Fig. 9(right)) decreases to a value $\beta_2 = \arccos(6\cos\alpha_2) \simeq 0.249298$ so that $\beta_2 = \arcsin(\frac{1}{4}\sin\alpha_2)$, then L increases by a factor of 6, while d decreases by the same factor of about 4.

Figs. 10–12 show the results of the simulations compared with experimental results, where Tables 1 and 2 present these results in numeric form. In Fig. 10, the longitudinal conductivity is plotted as function of n, for various temperature and stretching conditions. Figs. 11 and 12 show the conductivity ratios vs n.

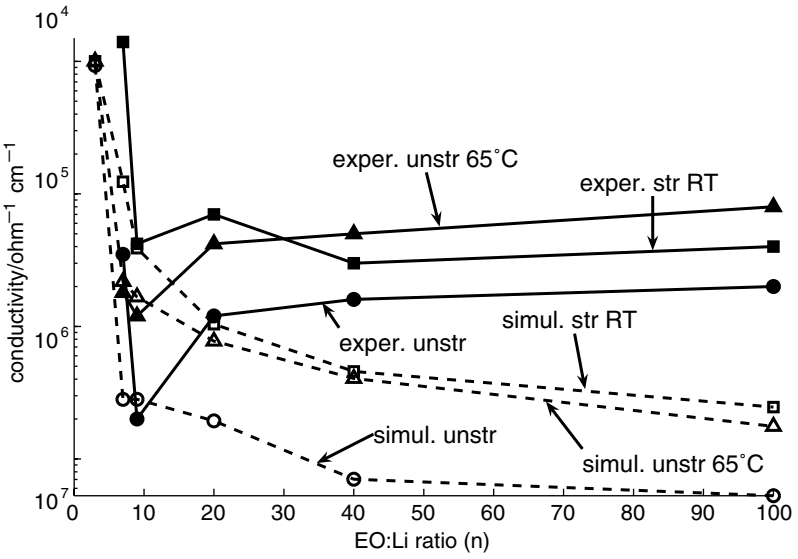

Fig. 10. Experimental and simulated longitudinal conductivity for different n. Experimental stretching was carried out at 60 °C. The longitudinal conductivity was measured after cooling of the stretched film to room temperature.

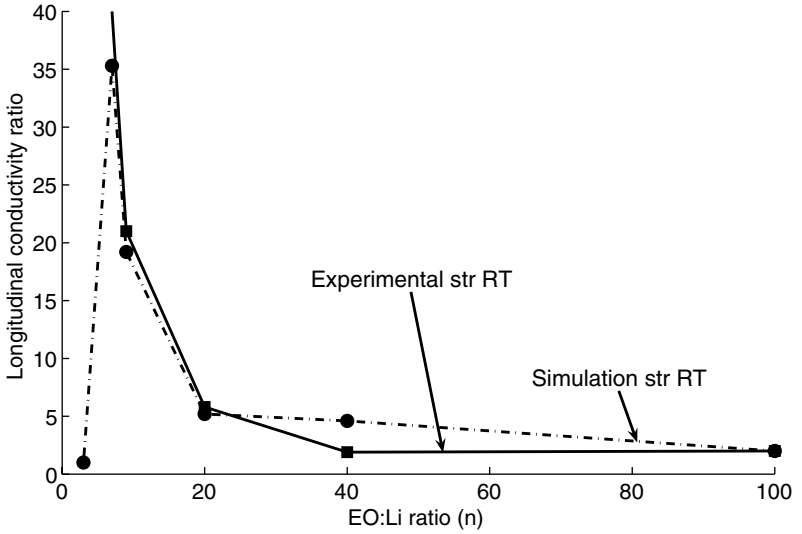

Fig. 11. Simulation/experimental conductivity ratios for different n. It shows the effect of stretching on the conductivity. The plots are conductivity ratio vs n. The films stretched at 60 °C. The longitudinal conductivity was measured after cooling of the stretched film to room temperature.

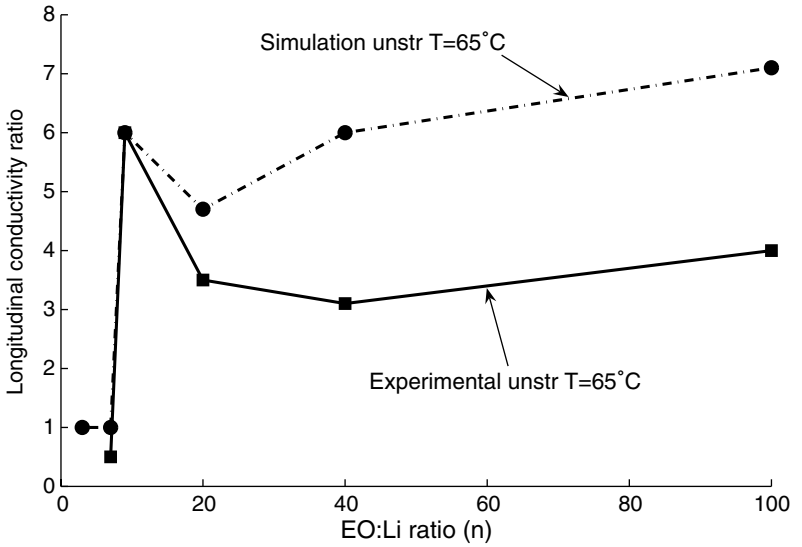

Fig. 12. Simulation/experimental conductivity ratios for different n showing the effect of the temperature for unstretched LiI:P(EO)n.

Table 1
Effect of stretching on the longitudinal conductivity of LiI:P(EO)n solid polymer electrolytes (SPE)

EO:Li ratio (n)	Simulation results			Experimental results [7,8]		
	Unstr. σ (S/cm) $\times 10^{-6}$	Str. σ (S/cm) $\times 10^{-6}$	$\sigma_{str}/\sigma_{unstr}$ ratio	Unstr. σ (S/cm) $\times 10^{-6}$	Str. σ (S/cm) $\times 10^{-6}$	$\sigma_{str}/\sigma_{unstr}$ ratio
3	92.9	100	1.1			
7	1.9	67	35.3	2.6	100	38.0
9	0.25	4.8	19.2	0.4	4.3	12.0
20	0.19	1	5.3	1.0	7.0	7.0
40	0.11	0.51	4.6	1.6	2.9	1.8
100	0.07	0.18	2.6	2.0	4.3	2.2

Table 2
Effect of temperature on the longitudinal conductivity of unstretched LiI:P(EO)n solid polymer electrolytes (SPE)

EO:Li ratio (n)	Simulation results			Experimental results [7,8]		
	σ at RT $\times 10^{-6}$	σ at $T = 65$ °C $\times 10^{-6}$	σ_T/σ_{RT} ratio	σ at RT $\times 10^{-6}$	σ at $T = 65$ °C $\times 10^{-6}$	σ_T/σ_{RT} ratio
3	92.9	94.5	1.0			
7	1.9	1.9	1.0	3.5	1.8	0.5
9	0.25	1.5	6.0	0.2	1.2	6.0
20	0.19	0.9	4.7	1.2	4.2	3.5
40	F 0.11	0.7	6.3	1.6	5	3.1
100	0.07	0.5	7.1	2	8	4.0

The effect of stretching on the longitudinal conductivity of LiI:P(EO)n solid polymer electrolytes (SPE) is given in Table 1.

The effect of temperature on the longitudinal conductivity of unstretched LiI:P(EO)n solid polymer electrolytes (SPE) is given in Table 2.

5. Discussion and conclusions

5.1. General

We note again the key simplifying assumptions in this model: Brownian dynamics of Li^+/I^- ions are simulated in a single molecule. In the present setup, the Li^+ and I^- ions are kept apart from each other by the polymer and the Li^+ ions are kept apart by Coulombic repulsion, so the finite size effects (e.g., Lennard-Jones forces) become significant only at high concentrations. Therefore, finite size effects are not incorporated in the present simulation. The polymeric film is a thin layer of molecular structures oriented at random. Each helix (molecule) forms a random angle with an axis (see Fig. 1), which is perpendicular to the electrodes. Upon mechanical stretching, the molecular structures align along the axis of stretching, i.e. the inclination of molecules decreases (see Fig. 9).

The limitations of our model result from its coarse-grained nature, as well as from the heuristic way in which we introduced the orientation of a molecule in space. This makes it difficult for a given material to assign volume fractions and local conductivities to existing phases. For this reason, we cannot hope to account quantitatively for any observation. Our aim was therefore to check whether the model introduced above can account for the qualitative observations in a consistent way.

5.2. Stretching effect

The simulation results of Fig. 11 show an excellent agreement in the effect of stretching on the longitudinal conductivity of PEO between simulation and experimental data over the entire n range. The agreement is not only in the correct trend (fast increase from $n = 3$ to $n = 9$, then an almost equally fast decrease from $n = 9$ to $n = 20$ with a further leveling of the ratios to an almost constant value), but also in the absolute values of the ratios. This in spite of the fact that the absolute values of the conductivities themselves, as seen in Fig. 10 and in Tables 1 and 2 match only at low n values. Above $n = 9$, the simulated vs. experimental longitudinal conductivity values for both RT stretched and unstretched PEO may differ by an order of magnitude and more. We note that the experimental values exhibit significant spreads [6–8]. In view of the uncertainly in these values, and the remark on the essentially qualitative nature of our model, the excellent agreement in conductivity ratios should be considered as indicative of a solid physical standing of the underlying physical model. The simulations certainly account for the qualitative observations.

5.3. Temperature effect

The agreement in the temperature effect on the PEO longitudinal conductivity shown in Fig. 12 is less impressive, with the correct trend seen only at low n values (1–20). Given the simplified model used in the

simulation, obtaining the correct trend as well as absolute ratio value over the entire n range (as in Fig. 11) or only over a partial n range (as in Fig. 12) is a significant achievement, which again attests to the fact that the model has solid physical standing.

Other assumptions made in our model remain to be tested by future experiments. Controlled measurements of the film conduction properties as functions of a properly chosen stretch parameter (angle of inclination) will be critical in this respect. In this context, it is important to mention again the differences that may exist between macroscopic and microscopic distortion. Macroscopic distortion always implies a change of shape. We assumed that such shape change takes place also on the microscopic molecular scale by changing the angle of inclination of the molecule, but one can envision a later stage of the stretch process in which the macroscopic shape changes due to redistribution of already elongated structural units in space, without further changes in their shape.

Acknowledgment

The first four authors were supported by a Grant 2004403 from the US–Israel Binational Science Foundation.

References

[1] M. Nathan, D. Haronian, E. Peled, Micro-electrochemical cell, U.S. Patent 6197450, 2001.
[2] M. Nathan, D. Golodnitsky, V. Yufit, E. Strauss, T. Ripenbein, I. Shechtman, S. Menkin, E. Peled, Three-dimensional thin-film microbatteries for autonomous MEMS, J. Microelectromech. Syst. 14 (5) (2005) 879–885.
[4] J.B. Kerr, in: G.-A. Nazri, G. Pistoia (Eds.), Lithium Batteries. Science and Technology, Kluwer Academic Press, Boston, 2004.
[5] O. Durr, W. Dieterich, P. Maass, A. Nitzan, Effective medium theory of conduction in stretched polymer electrolytes, J. Phys. Chem. B 106 (24) (2002) 6149–6155.
[6] D. Golodnitsky, E. Livshits, E. Peled, Highly conductive oriented polymer electrolytes, Macromol. Symp. 203 (2003) 27–45.
[7] D. Golodnitsky, E. Peled, E. Livshits, A. Ulus, Z. Barkay, I. Lapides, S.H. Chung, Y. Wang, S.G. Greenbaum, J. Phys. Chem., Part A 105 (2001) 10098–10106.
[8] D. Golodnitsky, E. Peled, E. Livshits, I. Lapides, Yu. Rozenberg, S.H. Chung, Y. Wang, S.G. Greenbaum, Solid State Ionics 147 (2002) 265–273.
[9] V. Kuppa, E. Manias, Computer simulation of PEO/layered-silicate nanocomposites: 2. Lithium dynamics in PEO/Li^+ montmorillonite intercalates, Chem. Mater. 14 (2002) 2171–2175.
[10] B. Hille, Ionic Channels of Excitable Membranes, Sinauer and Assoc., NY, 1993.
[11] R.S. Eisenberg, Ionic channels in biological membranes: electrostatic analysis of a natural nano-tube, Contemp. Phys. 39 (1998) 447–466.
[12] Z. Schuss, B. Nadler, R.S. Eisenberg, Derivation of PNP equations in bath and channel from a molecular model, Phys. Rev. E 64 (2–3) (2001) 036116-1–036116-14.
[14] Z. Schuss, Theory and Applications of Stochastic Differential Equations, Wiley, NY, 1980.
[15] A. Aabloo, J. Thomas, Solid State Ionics 143 (2001) 83–87.
[16] B.A. Ferreira, A.T. Bernardes, W.B. De Almeida, J. Mol. Struct. (Theochem) 539 (2001) 93–99.
[17] H. Tadokoro, Structural studies of several helical polymers, J. Polm. Sci. 15 (1966) 1–25.
[18] J.D. Jackson, Classical Electrodynamics, 2nd ed., Wiley, NY, 1975.
[19] H. Kramers, Brownian motion in a field of force, Physica (Utrecht) 7 (1940) 284.
[20] L. Greengard, V. Rokhlin, J. Comput. Phys. 73 (1987) 325.